Excited-state vibronic wave-packet dynamics in H_2 probed by XUV transient four-wave mixing

Wei Cao,[1] Erika R. Warrick,[2,3] Ashley Fidler,[2,3] Stephen R. Leone,[2,3,4] and Daniel M. Neumark[2,3]

[1]*School of Physics, Huazhong University of Science and Technology, Wuhan 430074, China*
[2]*Chemical Sciences Division, Lawrence Berkeley National Laboratory, Berkeley, California 94720, USA*
[3]*Department of Chemistry, University of California, Berkeley, California 94720, USA*
[4]*Department of Physics, University of California, Berkeley, California 94720, USA*

The complex behavior of a molecular wave packet initiated by an extreme ultraviolet (XUV) pulse is investigated with noncollinear wave mixing spectroscopy. A broadband XUV pulse spanning 12–16 eV launches a wave packet in H_2 comprising a coherent superposition of multiple electronic and vibrational levels. The molecular wave packet evolves freely until a delayed few-cycle optical laser pulse arrives to induce nonlinear signals in the XUV via four-wave mixing (FWM). The angularly resolved FWM signals encode rich energy exchange processes between the optical laser field and the XUV-excited molecule. The noncollinear geometry enables spatial separation of ladder and V- or Λ-type transitions induced by the optical field. Ladder transitions, in which the energy exchange with the optical field is around 3 eV, appear off axis from the incident XUV beam. Each vibrationally revolved FWM line probes a different part of the wave packet in energy, serving as a promising tool for energetic tomography of molecular wave packets. V- or Λ-type transitions, in which the energy exchange is well under 1 eV, result in on-axis nonlinear signals. The first-order versus third-order interference of the on-axis signal serves as a mapping tool of the energy flow pathways. Intra- and interelectronic potential energy curve transitions are decisively identified. The current study opens possibilities for accessing complete dynamic information in XUV-excited complex systems.

I. INTRODUCTION

When a molecule is exposed to an external extreme ultraviolet (XUV) field, dynamics with multiple degrees of freedom can be activated, leading to a complex wave packet including electronic, vibrational, and rotational motion. Studying the dynamics of such a wave packet is of great significance. First, if many electronic states excited by the coherent XUV pulse are closely spaced in energy, the associated electronic motion has a characteristic time scale comparable to that of the nuclear motion. Under such circumstances, the electronic and nuclear motion can be strongly coupled, and the Born-Oppenheimer (B-O) approximation starts to break down. Consequently, dynamical phenomena such as autoionization, predissociation, curve crossings, and conical intersections emerge [1–6]. Secondly, when an additional optical pulse is used to interrogate the evolution of the wave packet in a pump-probe geometry, the energy exchange between the electromagnetic field and the molecule will be imparted upon its nuclear and electronic degrees of freedom. This laser-driven electronic-nuclear correlation has attracted much attention recently [7–12]; it is a unique feature in molecular systems compared to atomic species, offering a promising tool for manipulating photochemical reactions. In this paper, the dynamics of an XUV-excited vibronic wave packet in a prototypical molecular system, H_2, is explored. The recently developed method of XUV-near-infrared (NIR) four-wave mixing spectroscopy [13,14] is applied to characterize the many pathways from the interaction of the NIR field with the XUV-excited state, probing such effects as laser-driven electronic-nuclear correlation and quantum coherence of the molecular wave packet.

There are many examples in which time-resolved photoion and photoelectron spectroscopies using high-order-harmonic-based XUV sources have been used to study highly excited wave packets in molecules [1–5,15–18]. The more recently developed technique of attosecond transient absorption spectroscopy (ATAS) offers complementary capabilities, as it is an all-optical technique that requires neither photoelectron nor photoion detection, and it can thus be applied to bound states lying below the ionization continuum. For example, ATAS using coaxial XUV and NIR laser pulses has revealed rich dynamic fingerprints in the transient absorption spectrum of molecules [19–25]. The measured result in ATAS is time resolved and energy resolved, a two-dimensional spectrogram [26]. Although this method holds the promise of completely characterizing the excited wave packet exposed to an optical laser pulse, the very congested energy levels and the multitude of quantum pathways pose great challenges for interpretation of the spectra. Multidimensional spectroscopies employing one or more XUV pulses have the potential to unravel this spectral complexity [27].

Recently, it has been shown that by crossing an XUV attosecond pulse with a NIR laser pulse at a small angle, nonlinear XUV-NIR four-wave mixing (FWM) from an atomic gas medium is observed at different emitting angles determined by the phase-matching conditions [13]. Under such a noncollinear geometry, ultrafast XUV spectroscopy gains an additional dimension that is angle resolved. This extra dimension can be utilized to successfully disentangle different transition pathways that appear at the same energy, offering a means to gain deeper insight into the associated physical
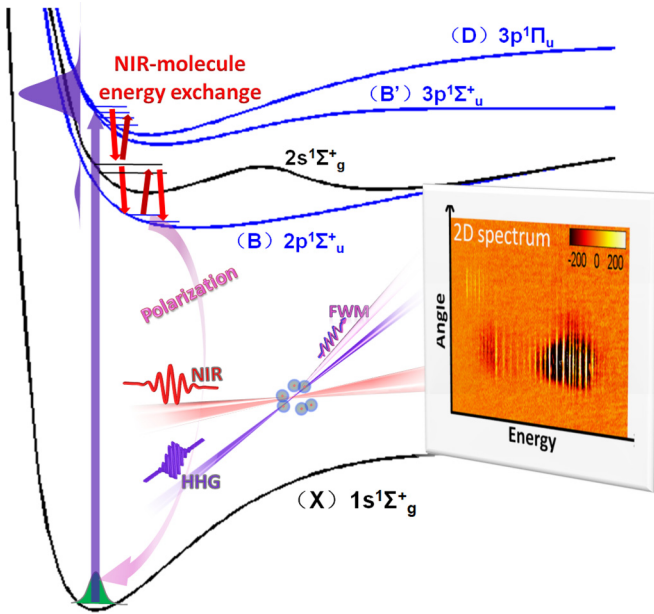
FIG. 1. Schematic of noncollinear transient wave mixing spectroscopy in H_2. The high-order-harmonics pulse (violet vertical arrow) promotes the molecule into a coherent superposition of multiple vibronic states in the np manifold. A delayed NIR pulse intersects with the HHG pulse at a crossing angle and drives transitions that are responsible for different energy flow pathways in the excited molecules. The laser-matter interaction induces a polarization dipole (purple arched arrow) that is detectable by a charge-coupled device (CCD) camera (inset). The energy flow pathway between the NIR pulse and molecules determines the direction of the transmitted XUV signal to conserve the momentum.

processes. In this paper, we apply this noncollinear transient wave mixing approach to study the response of electronically and vibrationally excited molecular hydrogen to an ultrafast NIR laser pulse and uncover the detailed energy exchange pathways between the NIR pulse and the vibronic wave packet initiated by the XUV pulse.

Figure 1 summarizes the principle of the experiment. The XUV pulse from high-harmonic generation (HHG) populates multiple potential energy curves (PECs), primarily the B' and D states, in H_2, from which a complex vibronic wave packet is formed that evolves freely. The coherence between the ground and excited electronic states forms a polarization dipole that can radiate XUV light. When the NIR pulse arrives first, the polarization in the XUV region is only a linear response induced by the harmonics. When the moderately intense NIR pulse arrives at or after the XUV pulse, it drives transitions between vibrational levels created by the XUV excitation. This action effectively builds up a nonlinear term in the polarization. This nonlinear term is predominantly a FWM process. By taking the difference between spectra with the NIR arriving first and NIR coinciding temporally with HHG, the laser-induced nonlinear response is captured as shown in the insets of Fig. 1. The molecules can either gain or lose energy during their interaction with the NIR pulse, and the energy flow direction depends on the sign of the net photon energy resulting from the two-NIR-photon transition. Due

to phase matching, the noncollinear configuration between the two mixing pulses spreads the XUV signals associated with different NIR-induced transitions at nonzero angles with respect to the XUV beam. Laser-driven V- or Λ-type transitions lead to a FWM signal emitting almost along the incident HHG propagation direction, while ladder-type transitions give rise to the background-free FWM signal at larger emission angles. By examining the individual transition pathways in a time-resolved manner, energy exchange dynamics between the optical laser field and the XUV-excited molecules can be extracted in great detail.

II. RESULTS

The experimental method is similar to that reported previously [13]. In brief, HHG is carried out in xenon gas using a sub-7-fs NIR pulse centered around 780 nm. The generated HHG spectrum is shaped by an indium filter to mainly contain the ninth harmonic ($\sim$15 eV) and a much weaker seventh harmonic ($\sim$12 eV). The shaped HHG field is thus an attosecond pulse train and its estimated duration is 2 fs. A replica of the few-cycle NIR pulse is picked off from the original pulse and intersects with the HHG pulse at an angle $\alpha \approx 12$ mrad; the value of the angle is calibrated based on the interference pattern of two NIR pulses as shown in [13]. In the interaction region, the NIR pulse has a beam size of about 250 μm and the peak intensity of the NIR pulse is estimated to be 1×10^{12} W/cm^2. The combined NIR and HHG pulses induce nonlinear wave mixing in the gas medium over a path length of about 1.5 mm, and the transmitted and emitted XUV spectrum after the medium is recorded by a high-resolution spectrometer with angular resolution.
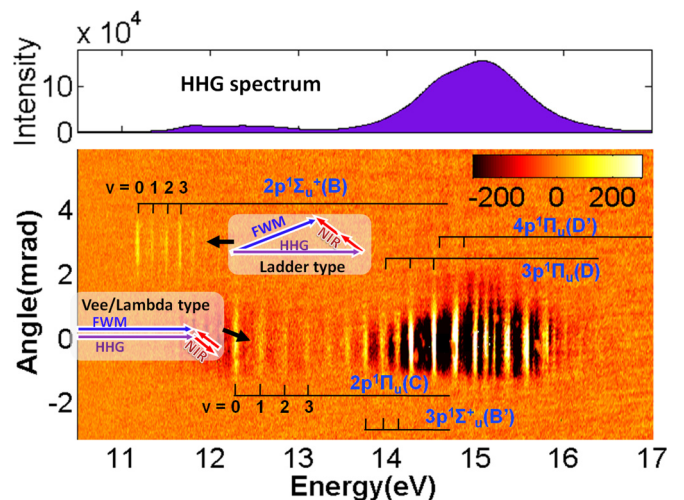

FIG. 2. A 2D image of the differential XUV spectrum versus angle after the nonlinear wave mixing in H_2 gas. The NIR pulse and the high-harmonic pulse overlap in time at a noncollinear angle. The differential spectrum is obtained by subtracting the spectrum with the negative time delay spectrum (NIR arrives first). The zero angle indicates the propagation direction of harmonics. The color scale indicates emission or absorption in arbitrary units. Phase-matching diagrams for ladder-type and Λ- or V-type transitions are also shown.
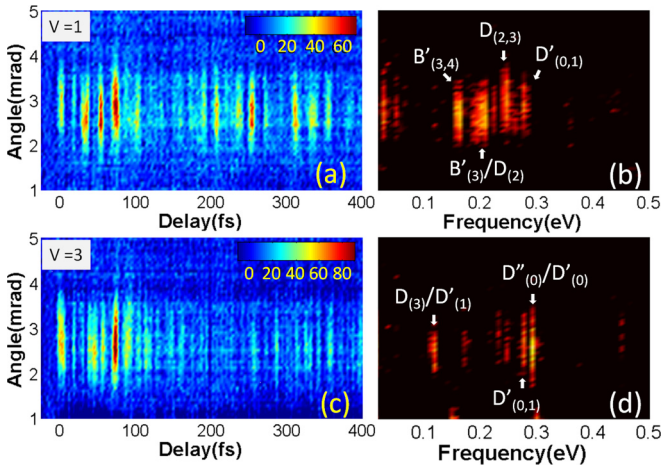
FIG. 3. Angle-resolved and time-resolved off-axis FWM signal for $v = 1$ (a) and $v = 3$ (c) on the B electronic state; the integration window for each vibrationally resolved FWM signal is about 0.05 eV. The delay step size is 1 fs. (b,d) are the Fourier transformations along the delay axis for $v = 1$ and $v = 3$, respectively.

FIG. 4. Absorption spectrum (optical density) of the on-axis signal as a function of time delay; positive delay means NIR arrives later.

Figure 2 shows the two-dimensional (2D) XUV differential spectrum when the NIR and XUV pulses are temporally overlapped. Extensive structure is seen both on and off axis, from Λ or V transitions and ladder transitions, respectively. The many vibronic levels activated by the XUV pulse overlap spectrally in the on-axis signal and thus can be only assigned partially.

The off-axis emission around $+3$ mrad in Fig. 2 is a background-free nonlinear signal from ladder-type transitions. The time-resolved and angle-resolved intensities of two off-axis emission lines corresponding to $v = 1$ (11.34 eV) and $v = 3$ (11.66 eV) of the B state are shown in Figs. 3(a) and 3(c). Some of these features are vertically displaced relative to others, an aspect that is discussed below. The corresponding Fourier spectra as functions of frequency (in eV) are shown in Figs. 3(b) and 3(d), respectively. The Fourier analysis provides two-dimensional information from which one can determine the states responsible for the various beat frequencies.

Figure 4 shows the delay-dependent absorption spectrum of the on-axis signals integrated over 1 mrad. This is similar to an attosecond transient absorption measurement except that ladder transitions are directed off axis by the phase-matching condition. The seventh and ninth harmonics induce polarizations associated with the B and Rydberg states, respectively. Common fingerprints in ATAS such as the energy shift or splitting at early delays due to the dynamic Stark effect, as well as the periodic modulations on various transition lines are clearly observed.

III. DISCUSSION

A. Off-axis FWM

According to the phase-matching diagram in Fig. 2, the emission angle θ of the nonlinear signals shown in Fig. 2 is proportional to the net energy exchanged Δ between the molecule and the NIR field, $\theta = \alpha \Delta / E$, where E is the energy of the state where the laser-driven transition ends [13]. The
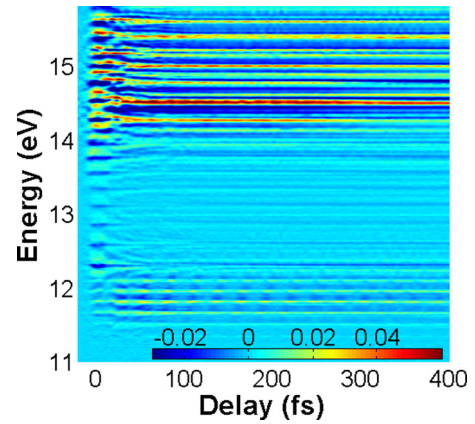
noncollinear wave mixing therefore projects the energy flow of laser-molecule interaction onto the emission angle, effectively separating the otherwise entangled transition pathways. The isolated signal appearing around 3 mrad is due to a 3.1 eV downward ladder-type energy exchange. It results from a transition from the vibrational levels at around 15 eV to the vibrational levels on the B state by stimulated emission of two NIR photons.

The time-resolved off-axis signal shown in Fig. 3 encodes the quantum coherence of the wave packet created by the XUV pulse onto the $v = 1$ and $v = 3$ levels of the B state. Because there are many pathways feeding into the same final state coherently, the intensity of the nonlinear signal shows delay-dependent modulations due to interference, which can be used to trace the quantum coherence of the molecular wave packet.

The limited bandwidth ($\sim$0.5 eV) of the NIR pulse sets constraints on the initial states (prepared by the XUV only) that can contribute to the FWM; i.e., the initial states must lie roughly 3.1 eV above the final state. For the $v = 1$ emission line (11.34 eV) the probed states lie around 14.45 eV, where the B', D, and D' states overlap [see Fig. 5(d)]. Thus this emission line is probing quantum coherence of a complex wave packet consisting of B', D, and D' states. The beat frequency alone is not always sufficient to unambiguously determine the involved states because of the congested energy levels in this region. The emission angle of the beat frequency is closely related to the mean energy E_m of the two states contributing to the beat signal by $\theta = \alpha(E_m - E_i)/E_m$, where E_i is the energy of the B-state vibrational level. Hence larger values of E_m lead to emission at larger θ, leading to the variations in the vertical displacements seen in Figs. 3(a) and 3(c).

We can pinpoint the sources for each beat frequency in Fig. 3(b) by combining both the observed angle and beat frequency. The two lower-frequency components (0.165 and 0.202 eV) with angle $\theta = 2.7$ mrad are from states around 14.4 eV. From the known energy levels, we can assign them as the vibrational coherence on B' ($v = 3$ and $v = 4$) and vibronic coherence between B' ($v = 3$) and D ($v = 2$), respectively. The two higher-frequency components (0.248 and 0.278 eV) with a slightly larger emission angle $\theta = 2.9$ mrad are from states

at 14.7 eV, and they are attributed to vibrational coherences on the D ($v = 2$ and $v = 3$) and D' ($v = 0$ and $v = 1$) states.

For the $v = 3$ emission line (11.66 eV), the probed initial states lie around 14.76 eV, where the wave packet consists of D, D', and D'' states. Following a similar analysis as for the $v = 1$ emission line, we can assign the quantum beats in Fig. 3(d), and they are indeed from vibrational levels belonging to D, D', and D''. The angles for $D_{(3)}/D'_{(1)}$ and $D''_{(0)}/D'_{(0)}$ beating components are predicted to be 2.57 and 2.52 mrad, respectively. These values are consistent with the experimental observations in Fig. 3(d), confirming our assignments. Therefore, the vibrationally resolved homodyne FWM is effectively an energetic tomography for probing dynamics by sectioning the wave packet along the energy axis, analogous to conventional geometric tomography.

B. On-axis FWM

Based on previous work on ATAS of Ar [30] and N_2 [20], the periodic modulations of various transition lines in Fig. 4 are attributed to first-order versus third-order quantum path interferences. The inverse of the modulation period is equal to the beat frequency of two states coupled by two NIR photons [19–21,30–33]. The absorption lines around 12 eV are mainly attributed to the B state. Each absorption line oscillates along the delay axis with a period that progressively increases with energy. Accordingly the energy difference of the adjacent vibrational levels coupled by two NIR photons decreases with energy. This regular oscillatory pattern is closely related to the anharmonic shape of a single PEC. In contrast, the absorption profile above 14 eV stems from many PECs that participate in the nonlinear process. The laser pulse can drive transitions either within the same or between different PECs, leading to a much more complex delay-dependent oscillation pattern.

Figure 5 is the Fourier transformation of Fig. 4. It shows the detailed beat frequency distribution of vibrational levels involved in the laser-driven transitions. The vibrationally resolved frequency distribution between 11 and 13 eV [see Fig. 5(a)] shows clear signatures of transitions on the B electronic state. Within its bandwidth ($\sim$0.5 eV), the few-cycle laser pulse can induce Raman-type transitions with Δv equal to 1, 2, and 3, corresponding to an energy exchange from 0.15 up to 0.45 eV. Each energy exchange group (i.e., $\Delta v = 1, 2, 3$) is bifurcated into two branches. In one branch, the final state lies above the initial state, corresponding to a positive energy flow where the molecule is gaining energy from the laser field, while in the other branch the energy flow direction is reversed. The cyan diamonds (white stars) are the predicted values for positive (negative) energy flow from the known vibrational energy levels, in good agreement with the experimental results. In this region, the energy exchange results solely from vibrational transitions.

The frequency distribution above 14 eV [Figs. 5(c), 5(e), and 5(f)] has a rather irregular pattern and encodes much more complicated dynamic information. The Franck-Condon factors from the ground state to the final states determine the possible involved PECs. The candidates include the $np\Sigma_u$ and $np\Pi_u$ molecular Rydberg states with $n \geqslant 3$. By examining the beat frequencies of these PECs carefully and comparing with the
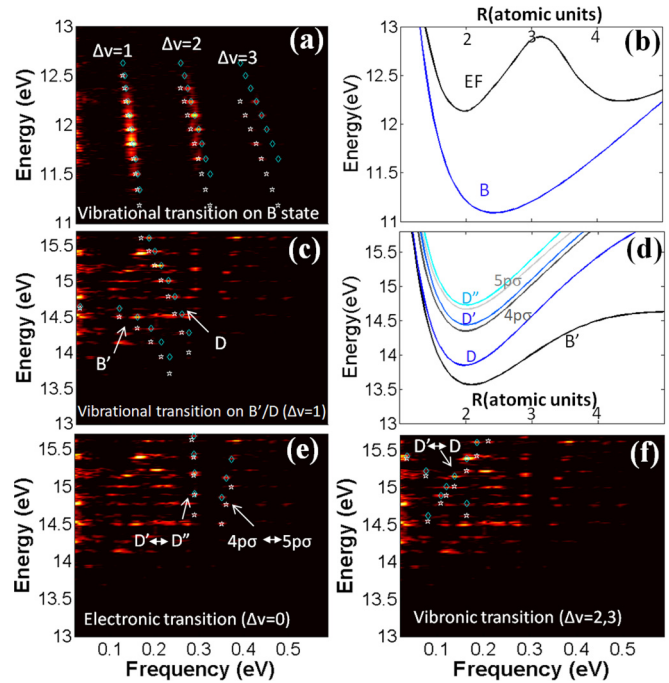

FIG. 5. Fourier analysis along the delay axis in the absorption spectrogram of Fig. 4, separated into low-energy (a) and higher-energy transitions (c,e,f). The coherences in panel (a) are from energy exchange between vibrational transitions of the B state. The energy exchange pathways in panels (c,e,f) involve the higher-lying Rydberg states and are more complex. They can involve only vibrational (c) or electronic transitions (e), or combinations of the two (f). The cyan diamonds (white stars) are the predicted values corresponding to the positive (negative) energy flow from the molecule to the laser field, respectively. The relevant PECs are shown in (b,d). The vibrational energy levels are adopted from Refs. [28,29,34].

measurement, we can break up the overall distribution into multiple distinct groups and assign them to different transition pathways. The pure vibrational transitions on the lowest Rydberg states $3p\sigma_u$ (B') and $3p\pi_u$ (D) can be recognized from their characteristic beat frequencies that line up with negative slopes [Fig. 5(c)], which is similar to Fig. 5(a). There is a second type of energy exchange pathway in which only the electron exchanges energy with the laser field. Such a process is indicated in Fig. 5(e). The beat frequencies at 0.29 eV are due to the laser-driven quantum transition between $4p\pi_u(D')$ and $5p\pi_u(D'')$ with $\Delta v = 0$ as predicted by the theoretical values. The similar shapes of the D' and D'' states indicate a negligible change of the nuclear position after the transition, and the molecules gain or lose energy by a pure electronic transition. This value (0.29 eV) is consistent with the asymptotic energy difference between D' and D''. From the experiment, we can also identify the signature of electronic transitions between $4p\sigma_u$ and $5p\sigma_u$ with beat frequencies around 0.35 eV. The diabatic $4p\sigma_u$ curve is strongly perturbed by the $(2s\sigma_u, 2p\sigma_u)$ doubly excited state and the ion-pair $H^+ + H^-(1s\sigma^2)$ state [35]. The perturbation deforms the shape of the diabatic $4p\sigma_u$ state. The slightly different shape between the $4p\sigma_u$ and $5p\sigma_u$ states leads to a larger value than 0.29 eV for transitions with $\Delta v = 0$.

A third type of transition pathway is shown in Fig. 5(f). The profound beat frequencies forming a crossing pattern are fingerprints of transitions between Rydberg states $3p\pi_u$ (D) and $4p\pi_u(D')$ with $\Delta v = 2$. They indicate vibronic transitions where both the electronic and vibrational levels change after the NIR laser-molecule interaction. The most pronounced beat frequency ($\sim$0.165 eV) is located at 15.388 eV ($v = 3$ state on D') in energy. It results from laser-induced population transfer from D ($v = 5$) to D' ($v = 3$). The D and D' states, with similar potential wells, are associated with the $3p$ and $4p$ electrons, respectively. The electron gains an energy of 0.6 eV (estimated from the asymptotic energy difference between D and D'), while the nuclei lose 0.44 eV (the energy difference between $v = 5$ and $v = 3$ vibrational levels on D' or D) during the interaction. This laser-driven energy correlation between the nuclei and electron leads to a net energy flow of $\sim$0.16 eV from the laser field to the molecule.

Each type of energy exchange pathway identified in Fig. 5 consists of two branches that represent the two opposite energy flow directions (cyan diamonds: positive; white stars: negative). In the current noncollinear beam experiment, the nonlinear signals associated with positive energy flow for which the molecule absorbs energy from the laser field are at a slightly negative emission angle, while that responsible for negative energy flow has a small positive emission angle. Although we select the on-axis signals centered at zero angle to reveal both processes simultaneously as shown in Fig. 5, the angle-resolved capability of the current spectroscopy allows us to spatially separate these two energy flows if the angular signals are isolated carefully. This indicates the possibility for accessing complete dynamic information of an excited molecular wave packet exposed to a laser field.

IV. CONCLUSIONS

The response of excited molecular hydrogen to an optical laser pulse is experimentally investigated using attosecond transient four-wave mixing spectroscopy. The vibronic wave packet prepared by attosecond pulses interacts with a time delayed laser pulse and energy exchange occurs between the optical field and the excited molecule. In the noncollinear experimental configuration, ladder transitions with energy exchanges of several electronvolts lead to off-axis nonlinear signals that are background free, and these signals are vibrationally resolved and encode quantum coherences of the molecular wave packet. Each vibrationally revolved FWM line probes a different part of the wave packet in energy, serving as a promising tool for energetic tomography of molecular wave packets. V and Λ transitions with energy exchanges of a fraction of an electronvolt lead to nearly on-axis nonlinear signals. The first-order versus third-order interference of the on-axis signal serves as a mapping tool of the energy flow pathways. Intra and inter PEC transitions are conclusively identified, revealing the complicated nature of the molecular wave packets. Such time-resolved, energy-resolved and angularly resolved XUV nonlinear spectroscopy reveals the possibility of accessing complete dynamical information of the laser-molecule interaction.

[1] A. Sandhu, E. Gagnon, R. Santra, V. Sharma, W. Li, Ph. Ho, R. Ranitovic, C. L. Cocke, M. M. Murnane, and H. C. Kapteyn, Science **322**, 1081 (2008).

[2] H. Timmers, N. Shivaram, and A. Sandhu, Phys. Rev. Lett. **109**, 173001 (2012).

[3] W. Cao, G. Laurent, I. Ben-Itzhak, and C. L. Cocke, Phys. Rev. Lett. **114**, 113001 (2015).

[4] X. Zhou, P. Ranitovic, C. W. Hogle, J. H. D. Eland, H. C. Kapteyn, and M. M. Murnane, Nat. Phys. **8**, 232 (2012).

[5] H. Timmers, Z. Li, N. Shivaram, R. Santra, O. Vendrell, and A. Sandhu, Phys. Rev. Lett. **113**, 113003 (2014).

[6] D. Sprecher, C. Jungen, W. Ubachs, and F. Merkt, Faraday Discuss. **150**, 51 (2011).

[7] H. H. Fielding, Annu. Rev. Phys. Chem. **56**, 91 (2005).

[8] J. Wu, M. Kunitski, M. Pitzer, F. Trinter, L. P. H. Schmidt, T. Jahnke, M. Magrakvelidze, C. B. Madsen, L. B. Madsen, U. Thumm, and R. Dorner, Phys. Rev. Lett. **111**, 023002 (2013).

[9] W. Zhang, Z. Li, P. Lu, X. Gong, Q. Song, Q. Ji, K. Lin, J. Ma, F. He, H. Zeng, and J. Wu, Phys. Rev. Lett. **117**, 103002 (2016).

[10] P. Lu, W. Zhang, X. Gong, Q. Song, K. Lin, Q. Ji, J. Ma, F. He, H. Zeng, and J. Wu, Phys. Rev. A **95**, 033404 (2017).

[11] C. B. Madsen, F. Anis, L. B. Madsen, and B. D. Esry, Phys. Rev. Lett. **109**, 163003 (2012).

[12] R. E. F. Silva, F. Catoire, P. Rivière, H. Bachau, and F. Martın, Phys. Rev. Lett. **110**, 113001 (2013).

[13] W. Cao, E. R. Warrick, A. Fidler, D. M. Neumark, and S. R. Leone, Phys. Rev. A **94**, 053846 (2016).

[14] W. Cao, E. R. Warrick, A. Fidler, S. R. Leone, and D. M. Neumark, Phys. Rev. A **94**, 021802 (2016).

[15] E. Gagnon, P. Ranitovic, X. Tong, C. L. Cocke, M. M. Murnane, H. C. Kapteyn, and A. Sandhu, Science **317**, 1374 (2007).

[16] K. P. Singh, F. He, P. Ranitovic, W. Cao, S. De, D. Ray, S. Chen, U. Thumm, A. Becker, M. M. Murnane, H. C. Kapteyn, I. V. Litvinyuk, and C. L. Cocke, Phys. Rev. Lett. **104**, 023001 (2010).

[17] G. Sansone, F. Kelkensberg, J. F. Pérez-Torres, F. Morales, M. F. Kling, W. Siu, O. Ghafur, P. Johnsson, M. Swoboda, E. Benedetti *et al.*, Nature **465**, 763 (2010).

[18] K. Ramasesha, S. R. Leone, and D. M. Neumark, Annu. Rev. Phys. Chem. **67**, 41 (2016).

[19] E. R. Warrick, J. E. Bækhøj, W. Cao, A. P. Fidler, F. Jensen, L. B. Madsen, S. R. Leone, and D. M. Neumark, Chem. Phys. Lett. **683**, 408 (2017).

[20] E. R. Warrick, W. Cao, D. M. Neumark, and S. R. Leone, J. Phys. Chem. A **120**, 3165 (2016).

[21] Y. Cheng, M. Chini, X. Wang, A. Gonzalez-Castrillo, A. Palacios, L. Argenti, F. Martin, and Z. Chang, Phys. Rev. A **94**, 023403 (2016).

[22] M. Reduzzi, W.-C. Chu, C. Feng, A. Dubrouil, J. Hummert, F. Calegari, F. Frassetto, L. Poletto, O. Kornilov, M. Nisoli, C.-D. Lin, and G. Sansone, J. Phys. B **49**, 065102 (2016).

[23] C. T. Liao, X. Li, D. J. Haxton, T. N. Rescigno, R. R. Lucchese, C. W. McCurdy, and A. Sandhu, Phys. Rev. A **95**, 043427 (2017).

[24] J. E. Bækhøj, L. Yue, and L. B. Madsen, Phys. Rev. A **91**, 043408 (2015).

[25] J. E. Bækhøj and L. B. Madsen, Phys. Rev. A **94**, 043414 (2016).

[26] A. R. Beck, D. M. Neumark, and S. R. Leone, Chem. Phys. Lett. **624**, 119 (2015).

[27] S. Mukamel, D. Healion, Y. Zhang, and J. D. Biggs, Annu. Rev. Phys. Chem. **64**, 101 (2013).

[28] U. Fantz and D. Wünderlich, At. Data Nucl. Data Tables **92**, 853 (2006).

[29] G. Staszewska and L. Wolniewicz, J. Mol. Spectrosc. **212**, 208 (2002).

[30] W. Cao, E. R. Warrick, D. M. Neumark, and S. R. Leone, New J. Phys. **18**, 013041 (2016).

[31] C. Ott, A. Kaldun, L. Argenti, P. Raith, K. Meyer, M. Laux, Y. Zhang, A. Blättermann, S. Hagstotz, T. Ding *et al.*, Nature **516**, 374 (2014).

[32] S. Chen, M. Wu, M. B. Gaarde, and K. J. Schafer, Phys. Rev. A **87**, 033408 (2013).

[33] A. R. Beck, B. Bernhardt, E. R. Warrick, M. Wu, S. Chen, M. B. Gaarde, K. J. Schafer, D. M. Neumark, and S. R. Leone, New J. Phys. **16**, 113016 (2014).

[34] S. Takezawa, J. Chem. Phys. **52**, 2575 (1970).

[35] M. Glass-Maujean, S. Klumpp, L. Werner, A. Ehresmann, and H. Schmoranzer, J. Chem. Phys. **126**, 144303 (2007).